

Exponential-sampling method for Laplace and other dilationally invariant transforms: II.  
Examples in photon correlation spectroscopy and Fraunhofer diffraction

This article has been downloaded from IOPscience. Please scroll down to see the full text article.

1991 Inverse Problems 7 21

(<http://iopscience.iop.org/0266-5611/7/1/004>)

View [the table of contents for this issue](#), or go to the [journal homepage](#) for more

Download details:

IP Address: 130.251.61.251

The article was downloaded on 21/04/2010 at 09:43

Please note that [terms and conditions apply](#).

# Exponential-sampling method for Laplace and other dilationally invariant transforms: II. Examples in photon correlation spectroscopy and Fraunhofer diffraction

M Bertero† and E R Pike‡

† Dipartimento di Fisica dell'Università di Genova and Istituto Nazionale di Fisica Nucleare, Via Dodecaneso 33, I-16146 Genova, Italy

‡ Department of Physics, King's College, London WC2R 2LS, UK and RSRE, Great Malvern WR14 3PS, UK

Received 11 September 1990

**Abstract.** The general theory of exponential sampling for the inversion of Mellin-type kernels presented in part I of this paper is applied to some practical inversion problems encountered in laser scattering experiments to determine particle size.

## 1. Introduction

Some years ago Ostrowsky *et al* [1] first introduced the exponential-sampling method for the inversion of the Laplace transform in photon correlation spectroscopy (PCS). This method relied on the conjecture that the nodes of the highest-index eigenfunctions used in a truncated eigenfunction expansion of the solution required were valid sampling points in the sense of a generalized Nyquist theorem. These eigenfunctions, calculated by McWhirter and Pike [2], show a geometric spacing of node positions.

The exponential-sampling method can be extended to the approximate solution of first-kind Fredholm integral equations of the following general type:

$$g(p) = \int_0^{+\infty} K(pt)f(t) dt \quad (1.1)$$

and in part I of this paper [3] we have shown that it can also be used for the approximate computation of the singular system of the following related integral equation

$$g(p) = \int_a^b K(pt)f(t) dt \quad (1.2)$$

where  $0 < a < b < +\infty$ . One example is the finite Laplace transform in the PCS problem.

The main mathematical difference between equations (1.1) and (1.2) is that, in the second case the integral operator is compact (under suitable integrability conditions on  $K(x)$ ) when the support of the unknown solution,  $[a, b]$ , is strictly positive and bounded. Therefore, while equation (1.1) can be diagonalized by means of the Mellin transform or, equivalently, by means of the generalized eigenfunctions introduced by

McWhirter and Pike [2], equation (1.2) can only be diagonalized by means of the singular system of the related integral operator. In part I we have introduced an exponential-sampling approximation of these singular functions. In this second part we give extensive applications to the practical inverse problems encountered in PCS and Fraunhofer diffraction, including integration of the data between sampling points and the 'zoom' method described in part I.

As concerns PCS and the monodisperse case of particle sizes, the normalized modulus of the first-order correlation function of the scattered electric field amplitude, such as the one measured directly in a heterodyne, quasi-elastic, light-scattering experiment (or extracted from an autodyne experiment), is given by [4]:

$$|g^{(1)}(\tau)| = \exp(-\Gamma\tau) \quad (1.3)$$

where  $\tau$  is the correlation delay time and

$$\Gamma = q^2 D \quad D = kT/6\pi\eta a. \quad (1.4)$$

Here  $q$  is the momentum transfer in the scattering experiment,  $D$  the linear diffusion coefficient,  $k$  the Boltzman constant,  $T$  the temperature,  $\eta$  the viscosity coefficient and  $a$  the equivalent spherical radius of the particles. The quantity  $\Gamma$  is also the characteristic linewidth of the (Lorentzian) optical spectrum associated with scattering from particles of radius  $a$ . Then, in the polydisperse case, the first-order correlation function is given by

$$|g^{(1)}(\tau)| = \int_0^{+\infty} \exp(-\tau\Gamma)G(\Gamma) d\Gamma \quad (1.5)$$

where  $G(\Gamma)$  is the normalized, linewidth-distribution function. The physical problem is the determination of  $G(\Gamma)$  from the measured values of  $|g^{(1)}(\tau)|$ . As follows from equation (1.4), the determination of  $G(\Gamma)$  is equivalent to the determination of the distribution function of the particle sizes,  $p(a)$ .

It is obvious that the problem (1.5) has exactly the structure of the problem (1.1) if we identify the variables as follows:  $\tau \rightarrow p$ ,  $\Gamma \rightarrow t$ ,  $|g^{(1)}(\tau)| \rightarrow g(p)$ ,  $G(\Gamma) \rightarrow f(t)$ . Moreover it is clear that we have

$$K(x) = \exp(-x) \quad (1.6)$$

and therefore this problem coincides with the inversion of the Laplace transform. The case (1.2), where the unknown distribution function has a bounded, strictly positive support was considered in [5, 6].

As concerns the problem of particle sizing by Fraunhofer diffraction, it is well known [7, 8] that the mean intensity per steradian diffracted by a random distribution of  $N$  opaque spherical particles is given, in the Fraunhofer region, by

$$I(\vartheta) = I_0 \sum_{i=1}^N \frac{a_i^2}{\vartheta^2} J_1^2(ka_i\vartheta) \quad (1.7)$$

where  $a_i$  is the radius of the particle  $i$ ,  $k$  is the wavenumber of the incident radiation and  $\vartheta$  is the scattering angle. This approximation is valid for small scattering angles

( $\vartheta \simeq \sin \vartheta$ ) and for radii of the particles sufficiently large with respect to the wavelength, more precisely when  $t = ka = 2\pi a/\lambda > 50$ . For smaller values of the variable  $t$  the Mie theory must be used. It has been shown, however, that the Mie result can be accurately reproduced in the forward region simply by adjusting the intensities without modifying the angular dependence [9]. With these modifications, called Mie corrections, the Fraunhofer kernel can be used down to values of  $t \gtrsim 1$ .

In the limit of a continuous distribution of radii  $p(a)$ , equation (1.7) becomes

$$j(\vartheta) = \int_0^{+\infty} \frac{J_1^2(\vartheta ka)a^2}{\vartheta^2} p(a) da \quad (1.8)$$

where  $j(\vartheta) = k^2 I(\vartheta)/I_0$ . This equation has the form (1.1) if we identify the variables as follows:  $\vartheta \rightarrow p$ ,  $ka \rightarrow t$ ,  $j(\vartheta) \rightarrow g(p)$  and  $a^4 p(a) \rightarrow f(t)$ . A complete analysis of this case has been performed in [10, 11]. In this paper we consider the case ( $p = \vartheta$ ,  $t = a$ )

$$g(p) = j(p)/p \quad f(t) = t^3 p(t). \quad (1.9)$$

Then  $g(p)$  is proportional to the output of an annular detector (or segment of an annulus) while  $f(t)$  is proportional to the volume distribution of the particles. Moreover in equation (1.1) we have

$$K(x) = \frac{1}{x} J_1^2(x). \quad (1.10)$$

In section 2 we summarize the numerical method introduced in part I for the approximate computation of the singular system of the integral operator (1.2). Moreover we illustrate, by means of a numerical example, the improvement of the approximation with increasing sampling frequency of the solution. In section 3 we compute the singular spectrum for the PCS problem both in the case of ideal pointwise data and in the case of integrated data, while in section 4 we investigate inversion algorithms for the same problems. In the case of particle sizing by Fraunhofer diffraction, the singular systems for pointwise and integrated data are investigated in section 5 and the inversion algorithms are presented in section 6. Some impressive examples of the 'zooming' technique discussed in part I are presented both in section 4 and in section 6.

## 2. The numerical method

In part I of this paper we have discussed the exponential-sampling approximation for the computation of the singular system of the integral operator (1.2). This approximation can be described as follows: the data function  $g(p)$  is replaced by the expansion

$$\tilde{g}(p) = \sum_{n=1}^N g(p_n) s(\Omega_1; p/p_n) \quad (2.1)$$

where

$$s(\Omega_1; x) = \frac{1}{\sqrt{x}} \frac{\sin[\Omega_1 \ln(x)]}{\Omega_1 \ln(x)} \quad (2.2)$$

and

$$p_n = p_1 \delta_1^{n-1} \quad \delta_1 = \exp\left(\frac{\pi}{\Omega_1}\right) \quad (2.3)$$

$\Omega_1$  being the effective (Mellin) bandwidth of the data. The solution  $f(t)$  is similarly replaced by

$$\tilde{f}(t) = \sum_{m=1}^M f(t_m) s(\Omega_2; t/t_m) \quad (2.4)$$

where

$$t_m = t_1 \delta_2^{m-1} \quad \delta_2 = \exp\left(\frac{\pi}{\Omega_2}\right) \quad (2.5)$$

$\Omega_2 > \Omega_1$  being the effective bandwidth of the solution; finally the kernel is approximated by

$$\tilde{K}(p_n t) = \sum_{l=1}^M K(p_n t_l) s(\Omega_2; t/t_l) \quad (2.6)$$

and the approximate orthogonality condition

$$\int_a^b s(\Omega_2; t/t_m) s(\Omega_2; t/t_l) dt \simeq \frac{\pi t_m}{\Omega_2} \delta_{lm} \quad (2.7)$$

is used. The result is that the integral equation (1.2) is approximated by means of the following algebraic system

$$b_n = \sum_{m=1}^M A_{nm}^{(N,M)} a_m \quad n = 1, \dots, N \quad (2.8)$$

where

$$b_n = \sqrt{\frac{\pi p_n}{\Omega_1}} g(p_n) \quad a_m = \sqrt{\frac{\pi t_m}{\Omega_2}} f(t_m) \quad (2.9)$$

and

$$A_{nm}^{(N,M)} = \frac{\pi}{\sqrt{\Omega_1 \Omega_2}} \sqrt{p_n t_m} K(p_n t_m). \quad (2.10)$$

When the matrix  $A_{nm}^{(N,M)}$  has been determined, its singular system can be computed by means of standard singular value decomposition (SVD) routines. We will denote by  $\{\alpha_k^{(N,M)}; U_k^{(N,M)}, V_k^{(N,M)}\}$  its singular system. We notice that the singular vectors  $U_k^{(N,M)}$  and  $V_k^{(N,M)}$  are normalized to unity with respect to the usual Euclidean norm. Then thanks to equations (2.4) and (2.9), the corresponding approximations of the singular functions  $u_k^{(N,M)}(t)$  of the integral operator (1.2) are given by

$$u_k^{(N,M)}(t) = \sum_{m=1}^M \sqrt{\frac{\Omega_2}{\pi t_m}} U_{k,m}^{(N,M)} s(\Omega_2; t/t_m) \quad (2.11)$$

where  $U_{k,m}^{(N,M)}$  is the  $m$ th component of the vector  $U_k^{(N,M)}$ .

The sampling points (2.3) are characterized by the two parameters  $\{p_1, \delta_1\}$  and analogously the sampling points (2.5) are characterized by the two parameters  $\{t_1, \delta_2\}$ .

The choice of the parameters  $\{p_1, \delta_1\}$  depends both on the structure of the kernel  $K(x)$  and on the support  $[a, b]$  of the unknown solution. The choice of the parameters  $\{t_1, \delta_2\}$  depends essentially on the support of the solution for a given value of  $M$ . As shown in part I, one possible choice is

$$\delta_2^{M-1} = \gamma \quad t_m = a\delta_2^{m-1} \quad m = 1, \dots, M. \tag{2.12}$$

where

$$\gamma = b/a. \tag{2.13}$$

We will show in a moment, by means of a numerical example, that a more convenient choice is the second one introduced in part I, namely

$$\delta_2^M = \gamma \quad t_m = a\delta_2^{m-1/2} \quad m = 1, \dots, M. \tag{2.14}$$

The difference between the two choices is obvious: in the second case all the sampling points are interior to the support  $[a, b]$  and the dilation factor  $\delta_2$  is slightly smaller than in the first case. Moreover, when  $M$  is odd,  $M = 2L + 1$ , the central point of the distribution (2.14), which corresponds to  $m = L + 1$ , coincides with the geometric mean of  $ab, \sqrt{ab}$ . As a consequence the distribution of these points is dilationally symmetric with respect to  $\sqrt{ab}$ .

In order to test the method we consider the following problem, investigated in [6], namely the inversion of the finite Laplace transform with discrete data

$$(Af)(p_n) = \int_1^\gamma \exp(-p_n t) f(t) dt \tag{2.15}$$

the  $p_n$  being given by equation (2.3). In [6] an exact method for the computation of the singular values of this problem is used. Here we compare the results obtained by means of the matrix (2.10) with the results obtained in [6], in the case  $\gamma = 5$ , the sampling points  $p_n$ , equation (2.3), being specified by the following parameters

$$N = 5 \quad p_1 = 0.1363 \times 10^{-2} \quad \delta_1 = 5.5. \tag{2.16}$$

In the case of these data points we have computed the first three singular values using the method described in this paper. In table 1 we give the results obtained when the sampling points of the solution are given by equation (2.12) with  $a = 1, \gamma = b/a = 5$ .

**Table 1.** Comparison of the exact singular values of finite Laplace transform, in the case of discrete data, with the singular values obtained by means of the exponential-sampling method, using the sampling points given by equation (2.12). In brackets are the errors with respect to the exact values.

$k$	Exact	$M = 21$	$M = 41$	$M = 61$
0	$8.742 \times 10^{-1}$	$8.939 \times 10^{-1}$ (2.2%)	$8.841 \times 10^{-1}$ (1.1%)	$8.808 \times 10^{-1}$ (0.7%)
1	$1.915 \times 10^{-1}$	$2.044 \times 10^{-1}$ (6.7%)	$1.980 \times 10^{-1}$ (3.4%)	$1.958 \times 10^{-1}$ (2.2%)
2	$3.815 \times 10^{-2}$	$4.261 \times 10^{-2}$ (11.7%)	$4.039 \times 10^{-2}$ (5.9%)	$3.965 \times 10^{-2}$ (3.9%)

**Table 2.** Comparison of the exact singular values of finite Laplace transform, in the case of discrete data, with the singular values obtained by means of the exponential-sampling method, using the sampling points given by equation (2.14). In brackets are the errors with respect to the exact values.

$k$	Exact	$M = 21$	$M = 41$	$M = 61$
0	$8.742 \times 10^{-1}$	$8.742 \times 10^{-1}$	$8.742 \times 10^{-1}$	$8.742 \times 10^{-1}$
1	$1.915 \times 10^{-1}$	$1.913 \times 10^{-1}$ (0.15%)	$1.914 \times 10^{-1}$ (0.05%)	$1.914 \times 10^{-1}$ (0.05%)
2	$3.815 \times 10^{-2}$	$3.796 \times 10^{-2}$ (0.50%)	$3.810 \times 10^{-2}$ (0.13%)	$3.813 \times 10^{-2}$ (0.05%)

The agreement is rather good but not excellent. The values of  $\delta_2$  are:  $\delta_2 = 1.0838$  for  $M = 21$ ,  $\delta_2 = 1.04106$  for  $M = 41$  and  $\delta_2 = 1.02719$  for  $M = 61$ .

Much better approximations are obtained using the distribution of sampling points given by equation (2.14) and these results are given in table 2.

It may be seen that the agreement is already very good in the case of 21 sampling points. The values of  $\delta_2$  are:  $\delta_2 = 1.07965$  for  $M = 21$ ,  $\delta_2 = 1.040035$  for  $M = 41$  and  $\delta_2 = 1.026735$  for  $M = 61$ . Moreover, we see that the accuracy is increased by increasing the number of sampling points of the solution, in agreement with the result proved in the appendix of part I.

Also in part I the case of integrated data has been considered, namely the case where the data of the problem are given by

$$G_n = \int_{p_n}^{q_n} g(p) dp \quad n = 1, \dots, N. \quad (2.17)$$

Here the  $p_n$  are given again by equation (2.3) and the  $q_n$  are given by a similar expression

$$q_n = q_1 \delta_1^{n-1}. \quad (2.18)$$

In any case  $p_n < q_n \leq p_{n+1}$ . When  $q_n = p_{n+1}$ , full integration between adjacent sampling points is considered. This is the case we consider in the problem of Fraunhofer diffraction. In the PCS problem integrated data can have the form (2.17) only in the case of heterodyne detection.

Also the problem with integrated data can be reduced to the form (2.8) where now

$$b_n = \sqrt{\frac{\Omega_1}{\pi p_n}} G_n \quad a_m = \sqrt{\frac{\pi t_m}{\Omega_2}} f(t_m) \quad (2.19)$$

and

$$A_{nm}^{(N,M)} = \frac{\pi}{\sqrt{\Omega_1 \Omega_2}} \sqrt{\frac{t_m}{p_n}} \frac{p_1}{q_1 - p_1} \int_{p_n}^{q_n} K(t_m p) dp. \quad (2.20)$$

It is easy to verify that, if  $q_n - p_n \ll p_n$ , then the matrix (2.20) is approximately equal to the matrix (2.10). Moreover, the interpolation formula (2.11) for the singular functions in the object space is valid also in the case of integrated data.

### 3. Polydispersity analysis by PCS: the singular system

As discussed in the introduction, the basic problem in polydispersity analysis by means of the PCS technique is the inversion of the finite Laplace transformation

$$(Af)(p) = \int_a^b \exp(-pt) f(t) dt, \quad 0 < p < \infty. \quad (3.1)$$

In a given experiment, the parameters  $a, b$  ( $0 < a < b$ ) are respectively the lower bound and the upper bound of the characteristic linewidths of the particles which, as follows from equation (1.4), are inversely proportional respectively to the upper bound and to the lower bound of the equivalent spherical radii of the particles.

As proved in [5], the operator (3.1) is compact and its singular values depend only on the parameter  $\gamma$ , equation (2.13). Therefore it is convenient, by means of a change of variable, to transform the interval  $[a, b]$  into the interval  $[1, \gamma]$ , as in equation (2.18). In the case of discrete data, however, if  $\{p_1, p_2, \dots, p_N\}$  is the set of data points which is used in the case of the interval  $[1, \gamma]$ , then, in order to get the same singular values in the case of the interval  $[a, b]$ , with  $b = \gamma a$ , one must use the data points  $\{p_1/a, p_2/a, \dots, p_N/a\}$  and also use scaling factors  $a^{-1/2}, a^{1/2}$  respectively for the data and the solution. Moreover the sampling points  $\{t_1, t_2, \dots, t_M\}$  must be replaced by  $\{at_1, at_2, \dots, at_M\}$ . As a result of these transformations, the matrix elements (2.10) have the same values in the case of the old and of the new sampling points.

The matrix (2.10) corresponding to the integral operator (3.1) is

$$A_{n,m}^{(N,M)} = \frac{\pi}{\sqrt{\Omega_1 \Omega_2}} \sqrt{p_n t_m} \exp(-p_n t_m). \quad (3.2)$$

The dependence on  $\gamma$  is not explicitly indicated but it is implicitly contained in the sampling points  $p_n, t_m$ .

In order to verify the accuracy of the numerical approximation provided by the matrix (3.2), we have again considered the case  $\gamma = 5$  and we have compared the results obtained by means of the matrix (3.2) with accurate numerical results obtained in previous work [5].

As shown in section 2, a good choice of the sampling points of the solution is given by equation (2.14). Here we take  $a = 1$  while  $\delta_2$  is determined when the values of  $\gamma$  and  $M$  are given.

Regarding the choice of the data points, we first remark that the dilation factor  $\delta_1$  is related to the signal-to-noise ratio and is essentially independent of  $\gamma$ . It can be determined by means of the method indicated in [2, 4] where the following values are computed:  $\delta_1 = 2.44, 1.88, 1.63$ , corresponding respectively to  $E/\varepsilon = 10^2, 10^3, 10^4$ .

Given the dilation factor, the next step is to determine the range of the data points, let us say  $[p_1, p_N]$  (even if the number  $N$  of data points is not yet known). This range is related both to the signal-to-noise ratio and to the solution support  $[1, \gamma]$ . In fact the data function  $g(p)$  contains all the exponentials with decay factors between 1 and  $\gamma$ . We must require that these exponentials are well represented in the interval  $[p_1, p_N]$ . Since the most rapidly decaying exponential is  $\exp(-\gamma p)$  while the most slowly decaying exponential is  $\exp(-p)$ , we will require the following conditions:

$$\exp(-\gamma p_1) = 1 - \frac{\varepsilon}{E} \quad \exp(-p_N) = \frac{\varepsilon}{E}. \quad (3.3)$$

Once  $p_1, p_N$  have been determined and also the value of  $\delta_1$ , related to the signal-to-noise ratio  $E/\varepsilon$ , the number  $N$  of sampling points can be determined by means of equation (2.3) with  $n = N$ . We will choose  $N$  as the first integer greater than

$$\tilde{N} = 1 + \frac{\ln(p_N/p_1)}{\ln \delta_1}. \quad (3.4)$$

In the case  $\gamma = 5$  we have the following results:

$$\begin{array}{lllll}
 \text{(A)} & E/\varepsilon = 10^2 & N = 9 & p_1 = 0.201 \times 10^{-2} & \delta_2 = 2.44 \\
 \text{(B)} & E/\varepsilon = 10^3 & N = 18 & p_1 = 0.2001 \times 10^{-3} & \delta_2 = 1.88 \\
 \text{(C)} & E/\varepsilon = 10^4 & N = 28 & p_1 = 0.2 \times 10^{-4} & \delta_2 = 1.63
 \end{array} \quad (3.5)$$

and in the case  $\gamma = 100$  the following ones:

$$\begin{array}{lllll}
 \text{(A')} & E/\varepsilon = 10^2 & N = 13 & p_1 = 0.1005 \times 10^{-3} & \delta_2 = 2.44 \\
 \text{(B')} & E/\varepsilon = 10^3 & N = 22 & p_1 = 0.1 \times 10^{-4} & \delta_2 = 1.88 \\
 \text{(C')} & E/\varepsilon = 10^4 & N = 34 & p_1 = 0.1 \times 10^{-5} & \delta_2 = 1.63.
 \end{array} \quad (3.6)$$

We see that the main change is in the choice of the first data point, while the change in the number of sampling points from  $\gamma = 5$  to  $\gamma = 100$  is not very important.

In table 3 we give the results obtained using the set (C) of data parameters in the case  $\gamma = 5$ .

Table 3. Comparison of the first five exact singular values of the finite Laplace transform, in the case  $\gamma = 5$ , with the singular values obtained by means of the exponential-sampling method, using the data points given by the set (C) of equation (3.5) and for various values of  $M$ , equation (2.14). In brackets are the errors with respect to the exact values.

$k$	Exact	$N = 28, M = 21$	$N = 28, M = 41$	$N = 28, M = 61$
0	$8.751 \times 10^{-1}$	$8.751 \times 10^{-1}$ (—)	$8.751 \times 10^{-1}$ (—)	$8.750 \times 10^{-1}$ (0.01%)
1	$1.935 \times 10^{-1}$	$1.933 \times 10^{-1}$ (0.10%)	$1.934 \times 10^{-1}$ (0.05%)	$1.935 \times 10^{-1}$ (—)
2	$3.827 \times 10^{-2}$	$3.810 \times 10^{-2}$ (0.44%)	$3.823 \times 10^{-2}$ (0.10%)	$3.825 \times 10^{-2}$ (0.05%)
3	$7.434 \times 10^{-3}$	$7.337 \times 10^{-3}$ (1.30%)	$7.408 \times 10^{-3}$ (0.35%)	$7.422 \times 10^{-3}$ (0.16%)
4	$1.435 \times 10^{-3}$	$1.394 \times 10^{-3}$ (2.86%)	$1.424 \times 10^{-3}$ (0.77%)	$1.429 \times 10^{-3}$ (0.42%)

This example indicates the possibility of using the exponential-sampling method for the accurate computation of the singular values. It is obvious, however, that this method is not necessarily the best from the numerical point of view. The main interest is in practical applications where it can be important to obtain satisfactory results with a small number of points.

We consider again the case  $\gamma = 5$ . When  $E/\varepsilon = 10^2$  only the singular values greater than  $10^{-2}$  contribute to the truncated singular function expansion [5]. These are just the first three singular values and one can look for the approximate values which can be obtained using the set of parameters (A), equation (3.5). In table 4 we give some of the values we have obtained using several choices of the number of sampling points in the object support. We see that, even when this number is rather large ( $M = 61$ ) the approximation of the third singular value is not very good (2%). It is interesting however that with a much smaller number of sampling points ( $M = 9$ ) it is possible to obtain a similar approximation (4%).

We conclude that a satisfactory approximation for practical purpose can be obtained using nine sampling points both for the data and for the solution.

A similar result is obtained in the case  $E/\varepsilon = 10^3$ , using the set (B) of equation (3.5), i.e. 18 sampling points for the data. In such a case we have five singular

**Table 4.** The first three singular values of the finite Laplace transform, with  $\gamma = 5$ , obtained using the set (A), equation (3.5), of data parameters and various values of the number of object sampling points. In brackets are the errors with respect to the exact values (table 3).

$k$	Exact	$M = 21$	$M = 41$	$M = 61$
0	$8.744 \times 10^{-1}$ (0.08%)	$8.726 \times 10^{-1}$ (0.28%)	$8.724 \times 10^{-1}$ (0.3%)	$8.724 \times 10^{-1}$ (0.3%)
1	$1.851 \times 10^{-1}$ (4.3%)	$1.921 \times 10^{-1}$ (0.72%)	$1.928 \times 10^{-1}$ (0.4%)	$1.929 \times 10^{-1}$ (0.3%)
2	$2.792 \times 10^{-2}$ (27%)	$3.658 \times 10^{-2}$ (4.4%)	$3.735 \times 10^{-2}$ (2.4%)	$3.750 \times 10^{-2}$ (2.0%)

values greater than  $10^{-3}$  and these can be obtained using, for example, 21 sampling points for the solution, the relative error with respect to the exact singular values ranging from 0.03%, in the case of the first singular value, to 2%, in the case of the fifth singular value.

We have used the method for investigating the dependence on  $\gamma$  of the singular-value spectrum over a large range of values of  $\gamma$ . We have chosen four values of  $\gamma$  which are approximately in a geometric progression from  $\gamma = 5$  to  $\gamma = 100$ , i.e.  $\gamma = 5, 14, 37, 100$  and in all these cases a dilation factor  $\delta_2 = 1.0267$ . The number of sampling points in the object support is respectively  $M = 61, 100, 137, 175$ . For the data sampling points we have used the set C, equation (3.6). The results are shown in table 5.

**Table 5.** Singular values ( $> 10^{-3}$ ) of the finite Laplace transform for various values of  $\gamma$  in the range 5–100.

$k$	$\gamma = 5$	$\gamma = 14$	$\gamma = 37$	$\gamma = 100$
0	$8.751 \times 10^{-1}$	1.082	1.218	1.319
1	$1.935 \times 10^{-1}$	$3.666 \times 10^{-1}$	$5.238 \times 10^{-1}$	$6.682 \times 10^{-1}$
2	$3.825 \times 10^{-2}$	$1.112 \times 10^{-1}$	$2.019 \times 10^{-1}$	$3.041 \times 10^{-1}$
3	$7.422 \times 10^{-3}$	$3.307 \times 10^{-2}$	$7.628 \times 10^{-2}$	$1.354 \times 10^{-1}$
4	$1.428 \times 10^{-3}$	$9.773 \times 10^{-3}$	$2.863 \times 10^{-2}$	$5.988 \times 10^{-2}$
5	—	$2.879 \times 10^{-3}$	$1.072 \times 10^{-2}$	$2.641 \times 10^{-2}$
6	—	—	$4.004 \times 10^{-3}$	$1.163 \times 10^{-2}$
7	—	—	$1.493 \times 10^{-3}$	$5.113 \times 10^{-3}$
8	—	—	—	$2.247 \times 10^{-3}$

We notice that, as proved in [5, 6], for a given  $k$  the singular values are increasing functions of  $\gamma$ . In particular the first eigenvalue  $\alpha_0$  tends to the limiting value  $\sqrt{\pi} = 1.77245$  when  $\gamma \rightarrow \infty$ .

These results quantify the improvement in resolution due to the *a priori* knowledge of the support. In fact, in the case  $E/\varepsilon = 10^3$  the dilation factor is  $\delta_0 = 1.88$  (see [5]) and this corresponds to a number of resolution elements which, in the cases  $\gamma = 5, 14, 37, 100$  is respectively  $K_0 = 2.5, 4.2, 5.7, 7.3$ . From table 5 we deduce that, when a priori knowledge of the support is used, the number of resolution elements, for the same values of  $\gamma$  is  $K = 5, 6, 7, 9$  (i.e. the number of singular values greater than  $10^{-3}$ ).

Finally we consider briefly the case of integrated data. If we assume that the points  $q_n$  are given by

$$q_n = p_n + \rho(p_{n+1} - p_n) \quad 0 \leq \rho \leq 1 \quad (3.7)$$

then the matrix (2.23) is given by

$$A_{nm}^{(N,M)} = \frac{\pi}{\sqrt{\Omega_1 \Omega_2}} \frac{1}{\sqrt{t_n p_m}} \frac{1}{\rho(\delta_1 - 1)} [\exp(-t_m p_n) - \exp(-t_m q_n)]$$

$$= \frac{\pi}{\sqrt{\Omega_1 \Omega_2}} \frac{1}{\sqrt{t_n p_m}} \frac{\exp(-t_m p_n)}{\rho(\delta_1 - 1)} \{1 - \exp[-\rho(\delta_1 - 1)t_m p_n]\}. \quad (3.8)$$

If  $\rho(\delta_1 - 1)t_m p_n \ll 1$ , then

$$1 - \exp[-\rho(\delta_1 - 1)t_m p_n] \simeq \rho(\delta_1 - 1)t_m p_n \quad (3.9)$$

and we re-obtain the matrix (3.1).

In order to investigate the behaviour of the singular values in terms of the integration parameter  $\rho$ , we have considered the case  $\gamma = 100$ , using the data set ( $A'$ ) of equation (3.6), and 21 sampling points in the interval  $[1, 100]$ , i.e.  $\delta_2 = 1.2451971$ .

The results are shown in table 6. By comparing the first column of table 6 with the last column of table 5 we see that the choice of sampling points used in this case provides a satisfactory approximation of the singular values  $> 10^{-2}$ . Moreover, for a given  $k$  the singular values are decreasing function of  $\rho$ .

Table 6. Singular values of the matrix (3.8), in the case  $\gamma = 100$ , for various values of the integration parameter, including  $\rho = 0$ , i.e. the matrix (3.2). The data set ( $A'$ ), equation (3.6), is used and the object sampling points are given by equation (2.14) with  $M = 21$ .

$k$	$\rho = 0$	$\rho = \frac{1}{3}$	$\rho = \frac{2}{3}$	$\rho = 1$
0	1.318	1.188	1.096	1.025
1	$6.671 \times 10^{-1}$	$5.998 \times 10^{-1}$	$5.504 \times 10^{-1}$	$5.119 \times 10^{-1}$
2	$3.031 \times 10^{-1}$	$2.713 \times 10^{-1}$	$2.467 \times 10^{-1}$	$2.271 \times 10^{-1}$
3	$1.345 \times 10^{-1}$	$1.194 \times 10^{-1}$	$1.072 \times 10^{-1}$	$9.716 \times 10^{-2}$
4	$5.879 \times 10^{-2}$	$5.183 \times 10^{-2}$	$4.585 \times 10^{-2}$	$4.074 \times 10^{-2}$
5	$2.496 \times 10^{-2}$	$2.232 \times 10^{-2}$	$1.968 \times 10^{-2}$	$1.698 \times 10^{-2}$
6	$1.360 \times 10^{-2}$	$1.055 \times 10^{-2}$	$7.089 \times 10^{-3}$	$5.425 \times 10^{-3}$

As a consequence, for  $\rho > \frac{1}{3}$ , the singular values  $> 10^{-2}$  are 6 instead of 7 and therefore the integration between sampling points implies a loss of information, albeit not very important.

#### 4. Polydispersity analysis by PCS: reconstruction algorithms

In part I of this paper we have indicated several reconstruction algorithms based on the singular-function expansion of the solution. These algorithms essentially rely on a filtering of this expansion and some of them provide a nearly positive approximate solution in the case where the true solution is positive. Most of these filtering methods, however, imply a loss of resolution and therefore they are not convenient in the case of PCS where the number of significant singular values is rather small. For this reason we have mainly considered the case of a rectangular (top-hat) window, i.e. the case of truncated singular-function expansions, equation (6.6) of part I.

If we use the interpolated singular functions, as given by equation (2.11), then this regularized solution is given by

$$\tilde{f}_K^{(N,M)}(t) = \sum_{k=0}^K \frac{1}{\alpha_k^{(N,M)}} (\mathbf{b}, \mathbf{V}_k^{(N,M)}) u_k^{(N,M)}(t) \tag{4.1}$$

where  $\mathbf{b}$  is the data vector defined in equation (2.9) (or equation (2.19) in the case of integrated data) and  $K$  is the maximum value of the index of the singular values satisfying the condition

$$\alpha_k^{(N,M)} \geq \varepsilon/E. \tag{4.2}$$

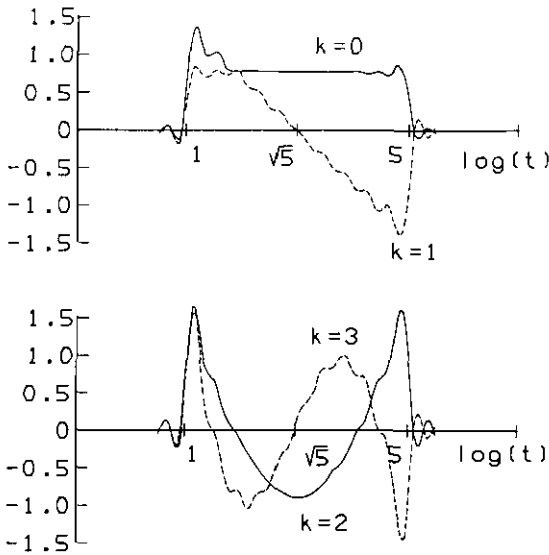


Figure 1. Plot of the first four singular functions  $u_k^{(N,M)}(t)$  in the case  $\gamma = 5$ . These have been computed using the set (A), equation (3.5), of data points and 21 sampling points in the solution support.

The first four of the corresponding singular functions are plotted in figures 1 and 2, respectively, in the cases  $\gamma = 5$  and  $\gamma = 100$ . More precisely in these figures we plot the functions

$$U_k^{(N,M)}(x) = \exp(x/2) u_k^{(N,M)}(\exp(x)) \tag{4.3}$$

the  $u_k^{(N,M)}(t)$  being given by equation (2.11). While the functions  $u_k^{(N,M)}$  are orthonormal in  $L^2(0, +\infty)$ , the functions  $U_k^{(N,M)}$  are orthonormal in  $L^2(-\infty, +\infty)$ . In the figures we indicate the value of the variable  $t = \exp(x)$ .

We notice that the singular functions  $U_k^{(N,M)}(x)$  are alternately even and odd with respect to the central point of the support in the  $x$ -variable. This corresponds to the geometric mean of the boundary points of the support in the  $t$ -variable. If we disregard

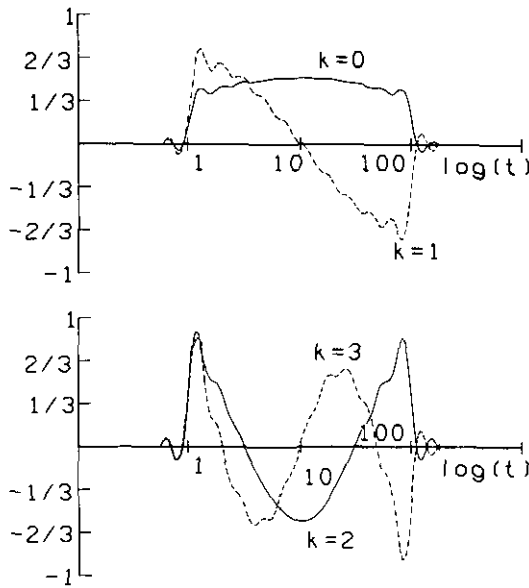


**Figure 2.** Plot of the first four singular functions  $u_k^{(N,M)}(t)$  in the case  $\gamma = 100$ . These have been computed using the set  $(A')$ , equation (3.6), of data points and 21 sampling points in the solution support.

the oscillations due to the interpolation by means of sinc functions, the behaviour of these singular functions is similar to the behaviour of the singular functions computed in [12].

The approximate solution (4.1) can be tested in the case where  $f(t)$  is a linear combination of delta functions or, in other words, in the case where the Laplace transform is a linear combination of exponentials

$$g(p) = \sum_{i=1}^J w_i \exp(-a_i p). \quad (4.4)$$

As shown in [6], in the case of single exponential (let us say  $w_1 = 1, a_1 = a$ ) the corresponding solution given by a truncated Mellin transform inversion is given by

$$\tilde{f}_\Omega^{(a)}(t) = \frac{\sin[\Omega \ln(t/a)]}{\sqrt{at} \pi \ln(t/a)} \quad (4.5)$$

where  $\Omega$  is the effective (Mellin) bandwidth. The value of this function at  $t = a$  is  $\Omega/\pi a$  while the ratio between the first zero to the right of  $t = a$  and  $a$  is given by  $\exp(\pi/\Omega)$ . Therefore the peak centred at  $a$  becomes smaller and broader when  $a$  increases. A similar behaviour is shown by the reconstruction of a delta function as provided by equation (4.1).

The difficulty was already indicated in part I, section 6, and it is not solved completely if the change of variable of equation (4.3) is used. In such a case the reconstruction of a delta function has a width (in the variable  $x = \ln t$ ) which does not depend on the position of the delta function but the height of the main peak still decreases when  $a$  increases. For this reason we will use the following change of variable

$$F(x) = \exp(x) f(\exp(x)). \quad (4.6)$$

The new function  $F(x)$  has the same integral as the old one

$$\int_a^b f(t) dt = \int_{\ln a}^{\ln b} F(x) dx. \quad (4.7)$$

Moreover, if we apply this transformation to the function (4.5) we get

$$\tilde{F}_\Omega^{(a)}(x) = \exp(x/2) \frac{\sin[\Omega(x - \ln a)]}{\sqrt{a}\pi(x - \ln a)} \quad (4.8)$$

and therefore the value of this function at  $x = \ln a$  is  $\Omega/\pi$ , independent of  $a$ .

The disadvantage of this transformation is that the oscillations of the solution are amplified for large values of  $x$  and this is an unpleasant effect in the case of PCS since one can use only a small number of singular functions and filtering techniques must be avoided. On the other hand this transformation is very convenient in the case of Fraunhofer diffraction as we will show in the next sections.

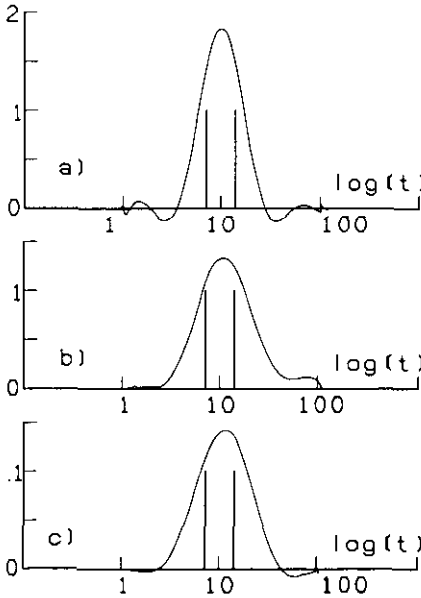


**Figure 3.** Reconstruction of two delta functions at  $t = 7$  and  $t = 14$  (both of weight 1) using the first nine singular functions corresponding to  $\gamma = 100$ ; (a) top-hat window; (b) triangular window; (c) Hanning window. The areas of the reconstructed functions are: (a) 2.00; (b) 2.13; (c) 2.05.

We conclude this section by showing one example of a reconstruction of a set of two delta functions. The data are given by equation (4.4) with  $a_1 = 7$ ,  $a_2 = 14$  (i.e.  $a_2/a_1 = 2$ ) and  $w_1 = w_2 = 1$ . We have first used the singular functions corresponding to the support  $[1, 100]$ , computed using the data set ( $C'$ ) of equation (3.6) (i.e. 34 data points) and 21 sampling points in  $[1, 100]$ . We have used all the singular values  $> 10^{-3}$ , i.e. nine singular values. The results are plotted in figure 3 where also the

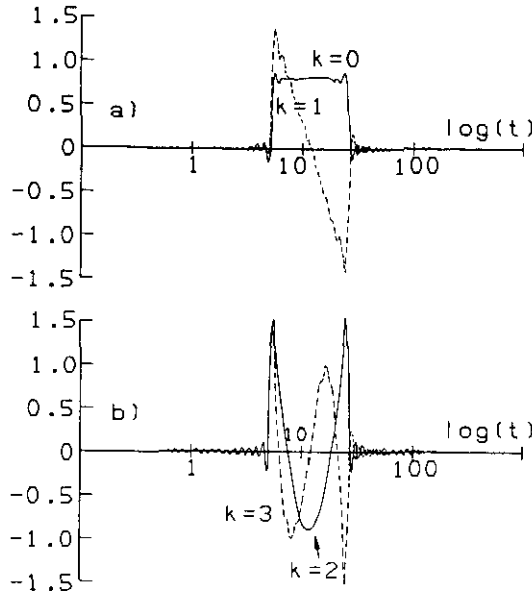


Figure 4. Plot of the first four singular functions corresponding to the support  $[5, 25]$ .

reconstructions provided by the triangular window and by the Hanning window (see part I, section 6) are given. As we see, the two delta functions are not resolved.

Then we have employed the 'zooming' effect discussed in part I, section 7. We have computed the singular system corresponding to the support  $[5, 25]$  using the same data points as in the previous case and 21 sampling points in  $[5, 25]$ . The singular values are essentially those given in the first column of table 5 and therefore we can use five singular functions if we accept all the singular values  $> 10^{-3}$ . The first four singular functions are plotted in figure 4. In figure 5 we plot the reconstructions obtained by means of this new singular system. We see that the two delta functions are now resolved if we use the 'top-hat' window while they are not yet resolved if we use the triangular or the Hanning window. In the last two cases, however, the solution is positive. Since the residual corresponding to these solutions is quite small this result seems to indicate that positivity does not have a beneficial effect on resolution. In fact, the reverse is the case.

## 5. Particle sizing by Fraunhofer diffraction: the singular system

As we discussed in the introduction, the integral equation we are considering now is given by equations (1.2), (1.10) and therefore the corresponding matrix (2.10) takes the following explicit form

$$A_{nm}^{(N,M)} = \frac{\pi}{\sqrt{\Omega_1 \Omega_2}} \frac{J_1^2(p_n t_m)}{\sqrt{p_n t_m}}. \quad (5.1)$$

It is interesting to point out that the physical situation described by (5.1) corresponds to measurement of the diffraction pattern by a set of  $N$  annular detectors

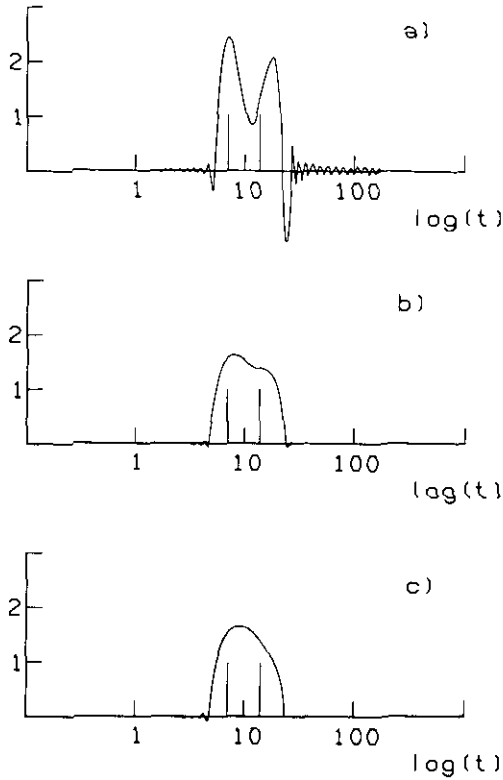


Figure 5. Reconstruction of the same delta functions of figure 3 using the first 5 singular functions corresponding to the support  $[5, 25]$  ( $\gamma = 5$ ). (a) top-hat window; (b) triangular window; (c) Hanning window. The areas of the reconstructed functions are: (a) 2.00; (b) 2.05; (c) 2.03.

placed at the sampling angles  $p_1, p_2, \dots, p_N$ , the angular size of each detector being negligible both with respect to  $(p_n - p_{n-1})$  and with respect to  $(p_{n+1} - p_n)$ . In practical situations, however, this approximation is not very useful since the detector integrates the diffraction pattern over a non-negligible interval  $[p_n, p_{n+1}]$ . In such a case, if  $N$  is the number of sampling points, the number of detectors is  $N - 1$  and the data are given by equation (2.17) with  $q_n = p_{n+1}$ . Moreover, equation (2.10) is replaced by equation (2.20).

In order to evaluate the integrals which appear in equation (2.20) when the kernel is given by equation (1.10), let us consider the following relation [13]:

$$\frac{1}{x} J_1^2(x) = -\frac{1}{2} \frac{d}{dx} [J_0^2(x) + J_1^2(x)]. \quad (5.2)$$

It follows that

$$\phi_n(t) = \int_{p_n}^{p_{n+1}} K(pt) dp = \frac{1}{2t} [J_0^2(p_n t) + J_1^2(p_n t) - J_0^2(p_{n+1} t) - J_1^2(p_{n+1} t)]. \quad (5.3)$$

Therefore, if we use the approximation

$$p_2 - p_1 = (\delta_1 - 1)p_1 \simeq \ln(\delta_1)p_1 \simeq \frac{\pi p_1}{\Omega_1} \quad (5.4)$$

from equation (2.20) we get the following matrix:

$$A_{nm}^{(N,M)} = \frac{1}{2t_m} \sqrt{\frac{\Omega_1 t_m}{\Omega_2 p_n}} [J_0^2(p_n t_m) + J_1^2(p_n t_m) - J_0^2(p_{n+1} t_m) - J_1^2(p_{n+1} t_m)] \quad (5.5)$$

the normalization of data and solution vectors being defined by equation (2.19). Let us remark that, both in equation (5.1) and in equation (5.5),  $N$  denotes the number of data sampling points so that the matrix (5.1) is  $N \times M$  while the matrix (5.5) is  $(N - 1) \times M$ .

In order to compare the singular-value spectra of these matrices, we have considered a situation which is typical of commercial instruments for particle sizing.

We have assumed a maximum angle of 10 deg, i.e.  $\vartheta_{\max} = 0.1745$  (in such a case the approximation  $\sin \vartheta \sim \vartheta$  is still rather good, since the maximum error is 0.5%) and a minimum angle of 0.076 deg, i.e.  $\vartheta_{\min} = 0.001328$ , so that  $\gamma = \vartheta_{\max}/\vartheta_{\min} \simeq 131$ . Moreover we have taken 31 sampling points with  $\vartheta_1 = \vartheta_{\min}$ ,  $\vartheta_{31} = \vartheta_{\max}$ ; the corresponding dilation factor is  $\delta_1 = 1.1766$ .

In order to determine the range of the radii of the particles we assume that  $\vartheta_{\max}$  corresponds to the maximum of the energy distribution of the smallest particles. Since in the variable  $x = \vartheta t$  this maximum occurs when  $x_{\max} = 1.375$ , we have  $t_{\min} = 7.88$ . Analogously we assume that  $\vartheta_{\min}$  corresponds to the maximum of the energy distribution of the largest particles. It follows  $t_{\max} = 1035$  and therefore  $\gamma = t_{\max}/t_{\min} \simeq 131$ . If we recall that  $t = ka$ , we see that  $t_{\min}$  is in the region where Mie corrections are required (see the introduction).

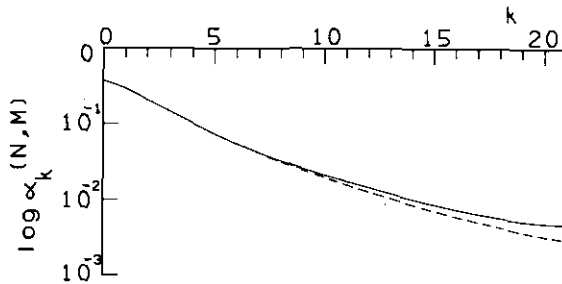


Figure 6. Singular-value spectra of the Fraunhofer problem both in the case of pointwise data (full curve) and in the case of integrated data (broken curve).

The distribution of the sampling points in the support  $[a, b] = [t_{\min}, t_{\max}]$  has been chosen according to the rule (2.14). For  $M = 21, 31, 51$  we have respectively  $\delta_2 = 1.262, 1.1704, 1.10038$ . In the cases  $M = 31$  and  $M = 51$  we have determined the number of singular values such that  $\alpha_0^{(N,M)}/\alpha_k^{(N,M)} < 100$ . This number is 23 in the case of the matrix (5.1) and 19 in the case of the matrix (5.5). Therefore integration between adjacent sampling points implies a loss of information (corresponding to a loss of resolution) of about 17%. This is in the case of a signal-to-noise ratio of the order of 100. If the signal-to-noise ratio is of the order of 300, then the number of relevant singular values is still 23 in the case of the matrix  $A$ , since  $\alpha_0^{(N,M)}/\alpha_{23}^{(N,M)} \sim 650$ , and it becomes just 23 in the case of integrated data. This result is quite interesting since

it implies that in the case of a very good signal-to-noise ratio the integration between adjacent sampling points does not imply a loss of resolution.

The singular spectra of the matrices (5.1) and (5.5) are plotted in figure 6.

We point out that the use of 23 singular functions implies the possibility of resolving 23 information elements in the interval  $[t_{\min}, t_{\max}]$ . This corresponds to a resolution factor  $\delta_{\text{res}} = 1.25$ , i.e. one can resolve two particles of radii  $a_1$  and  $a_2 > a_1$ , if  $a_2/a_1 > 1.25$ .

We do not plot the singular functions because their behaviour is quite similar to the behaviour of the singular functions of the PCS problem.

## 6. Particle sizing by Fraunhofer diffraction: reconstruction algorithms

It is obvious that, in the case of Fraunhofer diffraction, we can use the same reconstruction algorithms already used in the PCS problem. The main difference is that the number of significant singular values for the Fraunhofer problem is considerably greater than that for the PCS problem. For example in the case of a value of  $\gamma$  of the order of 100 we have only seven singular values greater than  $10^{-2}$  in the PCS problem while there are 18 in the Fraunhofer problem. As a consequence it can be convenient

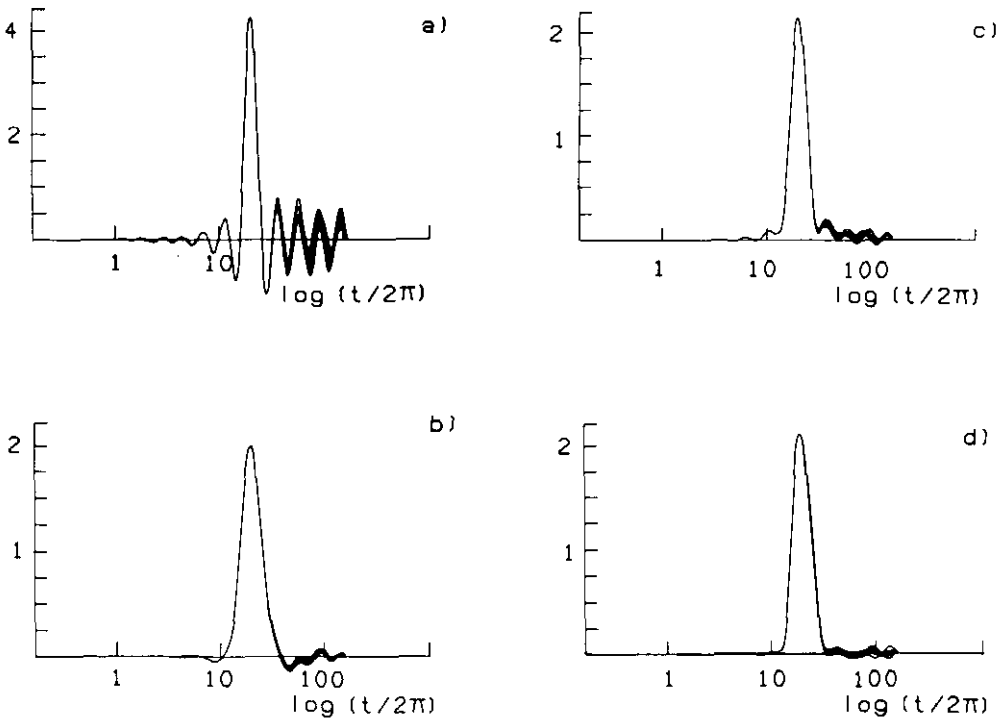


**Figure 7.** Reconstruction of a delta function at  $t/2\pi = 20$  using 18 singular functions: (a) top-hat window; (b) Tikhonov window with  $\alpha = 10^{-2}$ ; (c) triangular window; (d) Hanning window. In each figure we represent 10 different reconstructions corresponding to 10 different realizations of noise (1%).

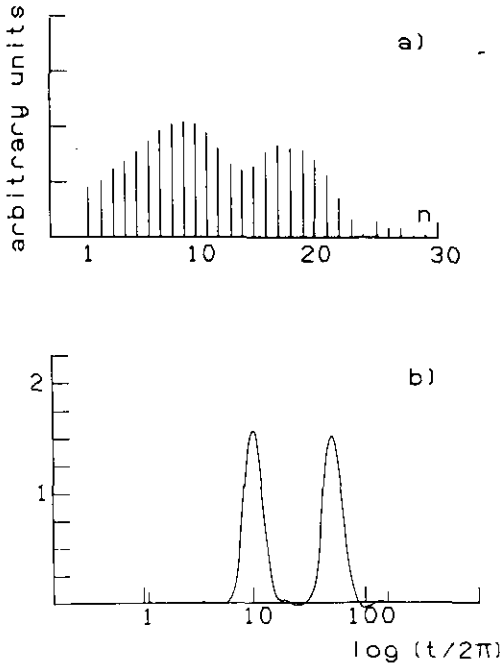


**Figure 8.** (a) Data vector (pointwise data) corresponding to a set of two delta functions having the same weight 0.75 and located at  $t_1/2\pi \approx 10$  and  $t_2/2\pi = 50$ . (b) Inversion of the data vector (a) using the Hanning window. The value of the integral of the restored function is 1.513.

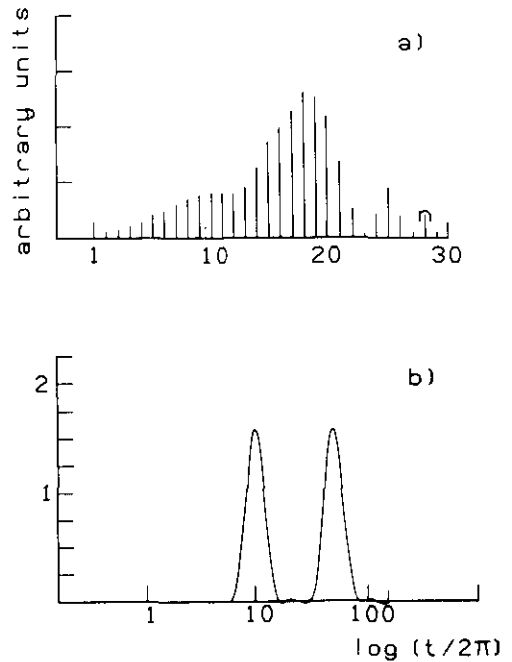


**Figure 9.** (a) Data vector (integrated data) corresponding to a set of two delta functions having the same weight 0.75 and located at  $t_1/2\pi = 10$  and  $t_2/2\pi = 50$ . (b) Inversion of the data vector (a) using the Hanning window. The value of the integral of the restored function is 1.510.

to use the filtering algorithms introduced in part I, section 6 even though their use can imply a loss of resolution.

Moreover we will use also in this section the transformation defined in equation (4.6).

In all the inversions of simulated data corresponding to a set of delta functions we have used the singular system obtained by means of 21 sampling points in the support  $[t_{\min}, t_{\max}]$ . In such a case we have 18 singular values such that  $\alpha_0^{(N,M)}/\alpha_k^{(N,M)} < 100$ , both for pointwise data and for integrated data. The data were perturbed by 1% random noise.

In figure 7 we plot the reconstruction of a delta function centred at  $t/2\pi = a/\lambda = 20$ . This means that the radius of the particles is 20 times the wavelength of the incident radiation. The reconstructions are plotted as functions of the variable  $\log(t/a)$ . We show the results obtained using top-hat, Tikhonov, triangular and Hanning windows. In each plot we give 10 different inversions corresponding to 10 different sequences of random noise. In such a way we give evidence of the numerical stability of the solution. Moreover we point out that the reconstructions obtained by means of the triangular and of the Hanning window are nearly positive, a property which was already pointed out in [14]. It can be seen that, in the case of the Hanning window, the sidelobes are rather small. For this reason in the following we will mainly use the Hanning window.

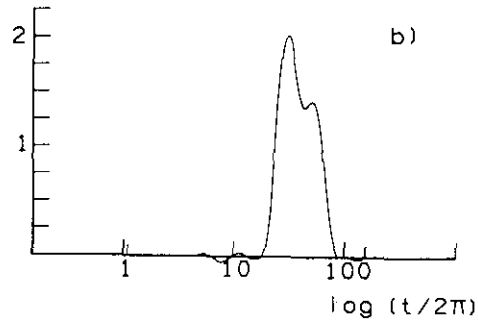
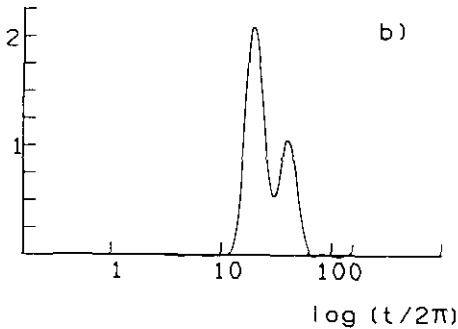
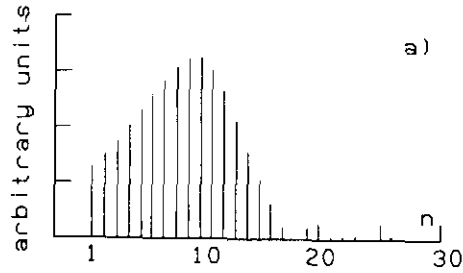
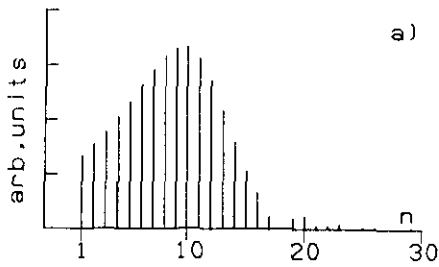


**Figure 10.** (a) Data vector (pointwise data) corresponding to a set of two delta functions located at  $t_1/2\pi = 20$  and  $t_2/2\pi = 40$ . The weight of the first is 1 while the weight of the second is 0.5. (b) Inversion of the data vector (a) using the Hanning window. The value of the integral of the restored function is 1.51.

**Figure 11.** (a) Data vector (pointwise data) corresponding to a set of two delta functions located at  $t_1/2\pi = 30$  and  $t_2/2\pi = 51$  ( $t_2/t_1 = 1.7$ ). The weight of the first is 1 while the weight of the second is 0.7. (b) Inversion of the data vector (a) by means of Hanning window. The value of the integral is 1.72.

In figures 8 and 9 we plot the reconstructions of the same set of two delta functions using, respectively, pointwise data and integrated data. The difference between the two reconstructions is negligible. In both cases the number of significant singular values, as defined above, is 18 and in both cases Hanning window was used.

In the example above the two delta functions are well separated (the ratio between their positions is 5) and this already appears from the behaviour of the data vector, at least in the case of pointwise data. This evidence is not so clear in the next example, given in figure 10. We give only the case of pointwise data because we have always found very small variations with respect to the restorations obtained with integrated data. In the example of figure 10, the ratio between the positions of the two delta functions is 2 and therefore it is still large with respect to the resolution limit corresponding to 18 singular functions, which is  $\delta_1 = 1.31$ . The best resolution limit achievable by means of the Hanning window is 1.7 and an example is shown in figure 11.

In order to improve this resolution it is necessary to use the 'zooming' technique discussed in part I of this paper. We give just one example showing that this procedure works also in the Fraunhofer case. We have considered two delta functions located at  $t_1/2\pi = 30$  and  $t_2/2\pi = 39$  so that  $t_2/t_1 = 1.3$ . Then we have computed the singular system corresponding to the interval  $[20, 50]$  in the variable  $t/2\pi$ . The corresponding value of  $\gamma$  is 2.5 and the number of significant singular values, i.e. such

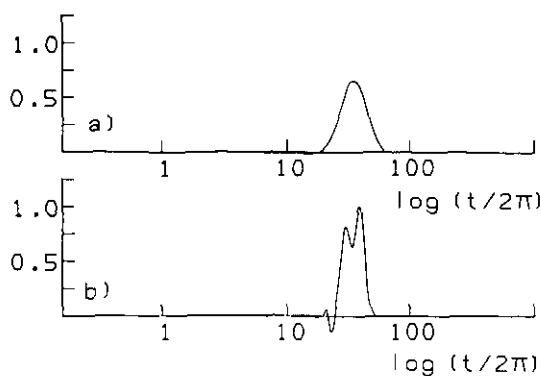


**Figure 12.** Inversion of the data corresponding to two delta functions at  $t_1/2\pi = 30$  and  $t_1/2\pi = 39$  ( $t_2/t_1 = 1.3$ ) both with weight 0.2: (a) inversion by means of the singular system corresponding to the support  $[1.25, 165]$  (18 singular functions); (b) inversion by means of the singular system of the support  $[20, 50]$  (9 singular functions). In both cases Hanning window has been used. The value of the integral is 0.403 in case (a) and 0.401 in case (b).

that  $\alpha_0^{(N,M)}/\alpha_k^{(N,M)} < 100$ , is 9. In figure 12 we compare the reconstruction obtained by means of Hanning window both in the case of the support corresponding to  $\gamma = 131$  and in the case of the support corresponding to  $\gamma = 2.5$ . In the last case the two delta functions are clearly resolved and the solution is still nearly positive.

## 7. Conclusion

In this paper we have applied the exponential-sampling method, implemented by singular-system analysis of part I, to PCS and Fraunhofer particle-sizing problems. The results show the limits of resolution which may be achieved in various practical cases.

## References

- [1] Ostrowsky N, Sornette D, Parker P and Pike E R 1981 Exponential sampling method for light scattering polydispersity analysis *Opt. Acta* **28** 1059-70
- [2] McWhirter J G and Pike E R 1978 On the numerical inversion of the Laplace transform and similar Fredholm integral equations of the first kind *J. Phys. A: Math. Gen.* **11** 1729-45
- [3] Bertero M and Pike E R 1990 Exponential-sampling method for Laplace and other dilationally invariant transforms: I. Singular-system analysis *Inverse Problems* **7** 1-20
- [4] Cummins H Z and Pike E R (ed) 1974 *Photon Correlation and Light Beating Spectroscopy* (New York: Plenum)
- [5] Bertero M, Boccacci P and Pike E R 1982 On the recovery and resolution of exponential relaxation rates from experimental data: I *Proc. R. Soc. A* **383** 15-29; 1984 On the recovery and resolution of exponential relaxation rates from experimental data: II *Proc. R. Soc. A* **393** 51-65
- [6] Bertero M, Brianzi P and Pike E R 1985 On the recovery and resolution of exponential relaxation rates from experimental data III *Proc. R. Soc. A* **398** 23-44
- [7] Shifrin K S and Perelman A Ya 1965 *Proc. 2nd Interdisciplinary Conf. on Electromagnetic Scattering (University of Massachusetts, June 1965)* ed R L Rowell and R S Stein (New York: Gordon and Breach)

- [8] Bayvel L P and Jones A R 1981 *Electromagnetic Scattering and its Applications* (London: Applied Science Publishers)
- [9] Fymat A L and Mease K D 1981 Mie forward scattering: improved semiempirical approximation with application to particle size distribution inversion *Appl. Opt.* **20** 194-8
- [10] Bertero M and Pike E R 1983 Particle size distributions from Fraunhofer diffraction: I. An analytic eigenfunction approach *Opt. Acta* **30** 1043-49
- [11] Bertero M, Boccacci P and Pike E R 1985 Particle size distributions from Fraunhofer diffraction: the singular value spectrum *Inverse Problems* **1** 111-26
- [12] Bertero M, Grünbaum A F and Rebolia L 1986 Spectral properties of a differential operator related to the inversion of the finite Laplace transform *Inverse Problems* **2** 131-9
- [13] Papoulis A 1968 *Systems and Transforms with Applications in Optics* (New York: McGraw-Hill) p 169
- [14] Bertero M Brianzi P Pike E R and Rebolia L 1988 Linear regularizing algorithms for positive solutions of linear inverse problems *Proc. R. Soc. A* **415** 257-75